

Connecting the Sun and the Solar Wind: The First Two-Dimensional Self-consistent MHD Simulation under the Alfvén Wave Scenario

Takuma Matsumoto and Takeru Ken Suzuki

Department of Physics, Nagoya University, Furo-cho, Chikusa-ku, Nagoya, 464-8602, Japan

takuma.matsumoto@nagoya-u.jp

ABSTRACT

We report the results of the first two-dimensional self-consistent simulations directly covering from the photosphere to the interplanetary space. We carefully set up grid points with spherical coordinate to treat Alfvénic waves in the atmosphere with the huge density contrast, and successfully simulate hot coronal wind streaming out as a result of surface convective motion. Footpoint motion excites upwardly propagating Alfvénic waves along an open magnetic flux tube. These waves, traveling in non-uniform medium, suffer reflection, nonlinear mode conversion to compressive modes, and turbulent cascade. Combination of these mechanisms, the Alfvénic waves eventually dissipate to accelerate the solar wind. While the shock heating by the dissipation of the compressive wave plays a primary role in the coronal heating, both turbulent cascade and shock heating contribute to drive the solar wind.

Subject headings: Sun: photosphere — Sun: chromosphere — Sun: corona — stars: mass-loss

1. Introduction

Although various mechanisms have been proposed, it is not still clearly explained why the hot corona exists above the cool photosphere and the high-speed solar wind emanates from there. The main difficulty arises from the rapid decrease of the density, amounting to more than 15 orders of magnitude. This huge density contrast has inhibited us to understand the energy transfer from the Sun to the solar wind as one system even within the magnetohydrodynamic framework.

Alfvénic wave is believed to be a reliable mechanism that drives the solar wind (e.g. McIntosh et al. 2011). Direct observations of propagating Alfvén waves have been successively reported after launch of Hinode satellite (De Pontieu et al. 2007; Nishizuka et al. 2008; Okamoto & De Pontieu 2011). Since its dissipation is a key, various processes have been explored. Recently, turbulent cascade is paid much attention; downward wave is generated by reflection in the stratified atmosphere, and Alfvénic turbulence is generated as a result of the interaction between the reflected wave and the pre-existing upward wave. The energy cascade of the turbulence finally heats the corona and drives the solar wind (Matthaeus et al. 1999). Phenomenological approaches that take into account the effect of turbulence have been often adopted to avoid complexities of turbulence (Cranmer et al. 2007; Verdini & Velli 2007). In numerical simulations the incompressible approximation is usually adopted (Dmitruk & Matthaeus 2003), although the mode conversion to compressive mode is also expected to be important (Kudoh & Shibata 1999; Suzuki & Inutsuka 2005, 2006; Antolin & Shibata 2010; Matsumoto & Shibata 2010). Moreover, the density decreases with more than 15 orders of magnitude from the solar photosphere to the interplanetary space. This huge

density contrast, which should largely affect the propagation of the Alfvén wave, has inhibited us to perform the direct numerical simulation from the Sun to the solar wind even within the magnetohydrodynamic (MHD) framework so far. In this paper we show results of first MHD simulation that can treat all these processes at once.

2. Method

We have performed two-dimensional MHD simulation with radiative cooling, thermal conduction, and gravity. Our numerical model includes a single flux tube extended from a kilo Gauss patch in the polar region (Tsuneta et al. 2008) to the interplanetary space (~ 20 Rs). Our basic equations are

$$\frac{\partial \rho}{\partial t} + \nabla \cdot (\rho \mathbf{V}) = 0, \quad (1)$$

$$\frac{\partial \rho \mathbf{V}}{\partial t} + \nabla \cdot \left(\rho \mathbf{V} \mathbf{V} + P_T - \frac{\mathbf{B} \mathbf{B}}{8\pi} \right) = \rho \mathbf{g}, \quad (2)$$

$$\frac{\partial \mathbf{B}}{\partial t} + \nabla \cdot (\mathbf{V} \mathbf{B} - \mathbf{B} \mathbf{V}) = 0, \quad (3)$$

$$\begin{aligned} \frac{\partial \mathcal{E}}{\partial t} + \nabla \cdot \left[(\mathcal{E} + P_T) \mathbf{V} - \frac{1}{4\pi} (\mathbf{V} \cdot \mathbf{B}) \mathbf{B} + \kappa \nabla T \right] \\ = \rho \mathbf{g} \cdot \mathbf{V} - R, \end{aligned} \quad (4)$$

where, ρ , \mathbf{V} , \mathbf{B} , T are mass density, velocity, magnetic field, temperature, respectively. P_T indicates total pressure, $P_g + B^2/8\pi$, where P_g is gas pressure. Total energy per unit volume is described as $\mathcal{E} = \rho V^2/2 + P_g/(\gamma-1) + B^2/8\pi$ with specific heat ratio $\gamma = 5/3$. \mathbf{g} is gravitational acceleration, $-GM/r^2 \hat{\mathbf{r}}$, where G , M are the gravitational constant and solar mass, respectively. We adopt anisotropic thermal conduction tensor κ along magnetic field lines (Yokoyama & Shibata 2001). Radiative cooling term R

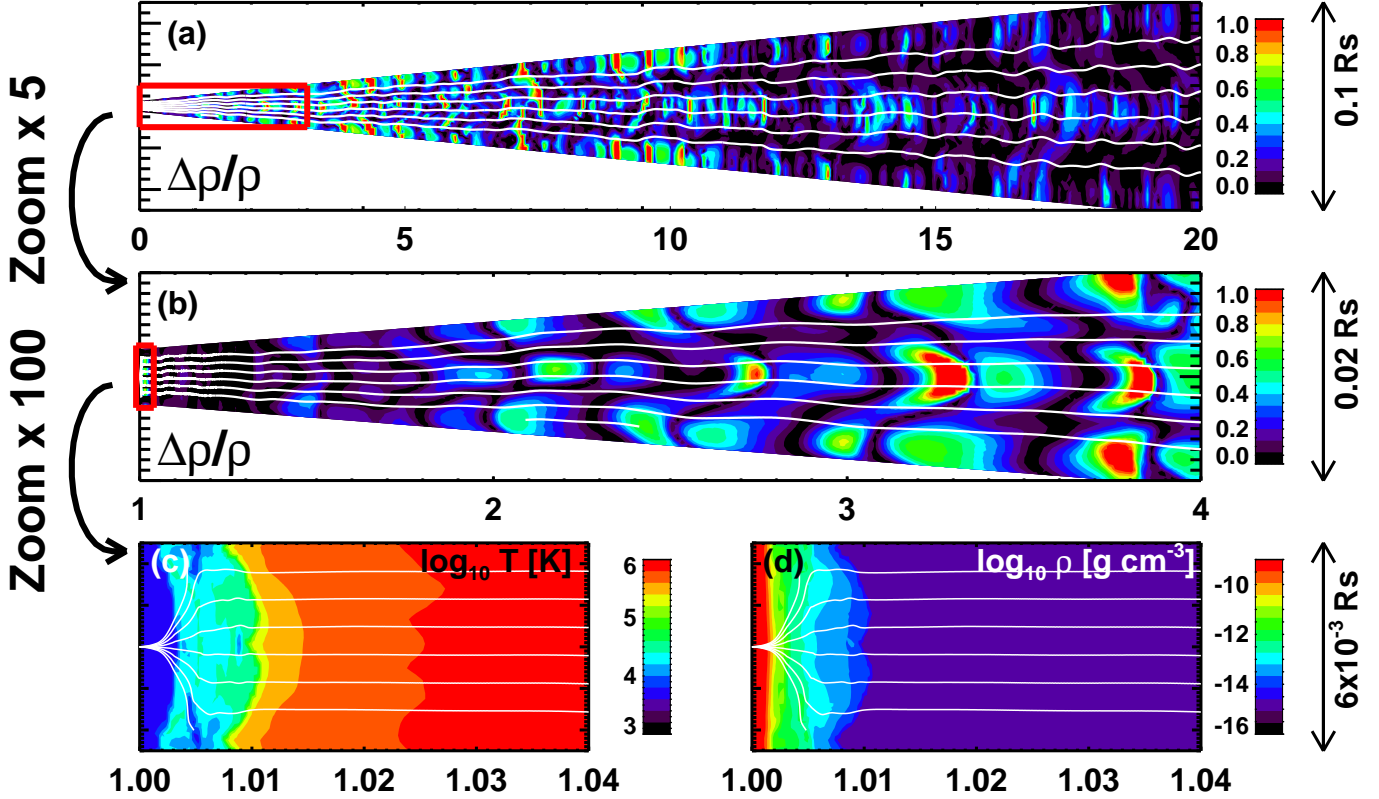


Fig. 1.— Results of MHD simulation of Alfvénic wave propagation from the photosphere to the interplanetary space. (a) The top panel shows the normalized density fluctuation $\Delta\rho/\rho$. (b) The middle panel also shows $\Delta\rho/\rho$ although the region is magnified 5 times from the top panel. The red squared region in the top panel is equivalent to the middle panel. The bottom right (c) and bottom left (d) panels show the temperature and density distribution, respectively, while the showing region is magnified 100 times from the middle panel. The red squared region in the middle panel is equivalent to the bottom panel. The white solid lines in each panel represent the magnetic field lines. All length units described in the figure is $R_s = 6.96 \times 10^5$ km.

is assumed to be a function of local density and temperature (Suzuki & Inutsuka 2005). Note that no other ad hoc heating source terms are included in the energy equation.

The vector form of our basic equations are appropriately transformed into spherical coordinate system with $(r, \theta = \pi/2, \phi)$ and $\partial_\theta = 0$. Initial magnetic field is extrapolated by using potential field approximation so that open field lines are extended from a kilo Gauss patch and decrease their strength to 10 Gauss at the height of 2,000 km. Initially, we set an isothermal (10^4 K) atmosphere. Alfvénic waves are driven by velocity disturbance in θ direction as boundary condition at the photosphere. We assume white noise power spectrum with $(1 \text{ km s}^{-1})^2$ in total power, which is rather good approximation to observed spectrum (Matsumoto & Kitai 2010). Periodic boundary condition is posed on ϕ direction. Our numerical scheme is based on HLLD scheme (Miyoshi & Kusano 2005) that is robust and efficient among the various kind of approximate Riemann solvers. The solenoidal condition $\nabla \cdot \mathbf{B} = 0$, is satisfied within a round-off error by using flux-CT method (Tóth 2000). The TVD-MUSCL scheme enables us to archive the second order accuracy in space, while the Runge-Kutta method gives the second order accuracy in time.

The turbulent heating rate is estimated by dimensional analysis since viscosity and resistivity are not included explicitly in our basic equations. First, we derive the Fourier component, \hat{v}_θ , of the Alfvénic disturbance (v_θ) as follows.

$$\hat{v}_\theta(r, k_\phi) = \int v_\theta(r, \phi) e^{-ik_\phi \phi} d\phi \quad (5)$$

Then, energy spectral density, $E(r, k_\phi)$, becomes

$$E(r, k_\phi) = \frac{1}{2\pi\Delta\phi} [|\hat{v}_\phi(r, k_\phi)|^2 + |\hat{v}_\phi(r, -k_\phi)|^2], \quad (6)$$

where $\Delta\phi$ indicates the angular system size in ϕ direction. By using k_ϕ and $E(r, k_\phi)$, we can estimate the energy exchanging rate, $\epsilon(r, k_\phi)$, for a certain wave number, k_ϕ , with neighboring Fourier modes.

$$\epsilon(r, k_\phi) \sim \bar{\rho} E(r, k_\phi)^{3/2} k_\phi^{5/2}, \quad (7)$$

where $\bar{\rho}$ denotes the mean density averaged over time and ϕ direction. As a turbulent heating rate, we use $\epsilon(r, k_\phi)$ whose wave number are larger than a critical wave number that is determined by numerical resolution. We choose $k_\phi \Delta\phi / 2\pi = 4$ as the critical wave number that corresponds to the spatial resolution covering one wave length by 8 grid points in our simulation.

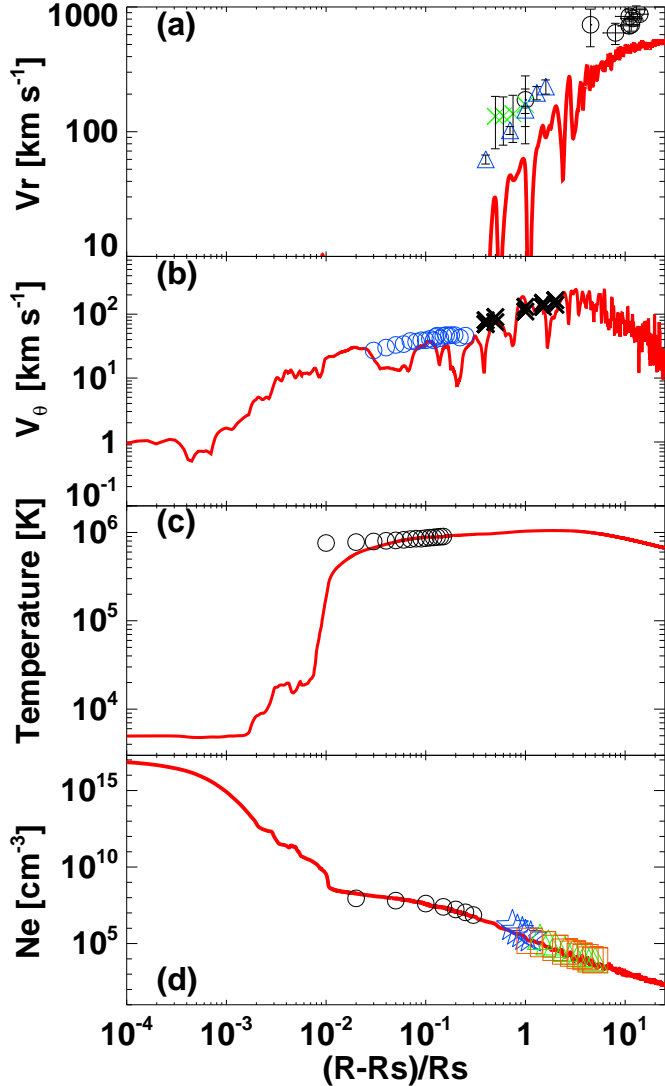


Fig. 2.— Comparison of the simulation and the observation summarized below. Red solid lines in each panels represents results of simulations; these values are averaged over direction spatially and over 30 minutes temporally. (a) The green crosses (Teriaca et al. 2003) and the blue triangles (Zangrilli et al. 2002) represent the proton outflow speeds in the polar region observed by SOHO. The black circles with crossed error bars (Grall et al. 1996) are obtained by VLBA. The black circles with vertical error bars (Habbal et al. 1995) indicate measurements by SPARTAN 201-01. (b) The blue circles (Banerjee et al. 1998) show the nonthermal broadening inferred from SUMER/SOHO. The black crosses (Esser et al. 1999) are empirically derived nonthermal broadening based on UVCS/SOHO measurements. (c) The black circles (Fludra et al. 1999) show electron temperature by CDS/SOHO. (d) The black circles (Wilhelm et al. 1998) and the blue stars (Teriaca et al. 2003) are data based on observations by SUMER/SOHO and by CDS/SOHO, respectively. The green triangles (Teriaca et al. 2003) and orange squares (Lamy et al. 1997) are observed by LASCO/SOHO.

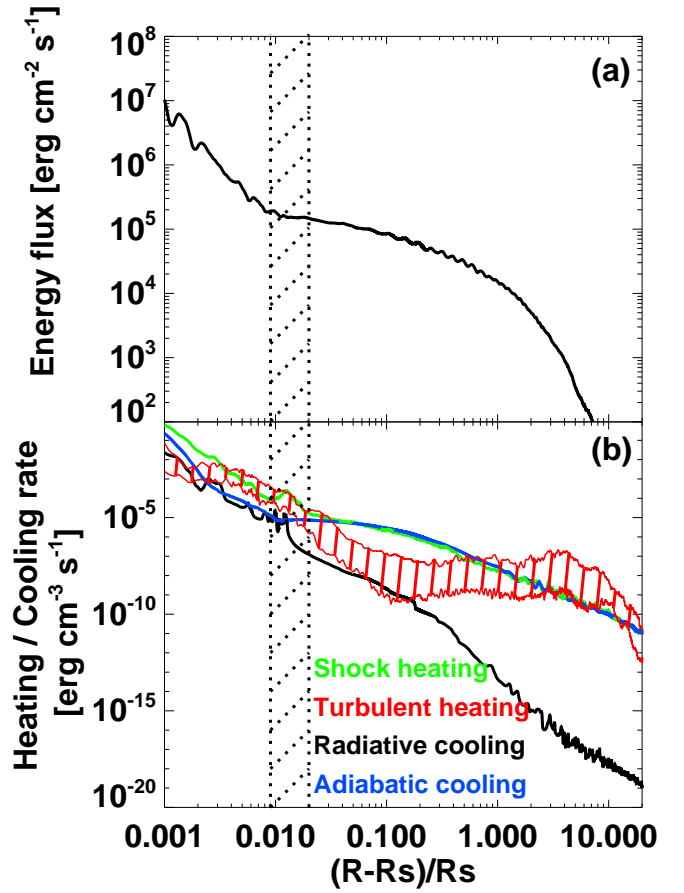


Fig. 3.— Alfvénic wave energy flux and its dissipation processes. (a) Alfvénic wave energy flux with respect to radius. (b) Heating and cooling rate with respect to radius. The green solid line shows shock-heating rate estimated by counting sudden entropy jumps. The red-hatched area indicates turbulent heating rate estimated by Fourier and dimensional analysis. The black solid line and the blue solid lines show radiative and adiabatic cooling rate respectively. The black-hatched area represents the transition region.

3. Results & Discussions

The coupling between the magnetic field and the surface convection excites upward propagating Alfvénic wave (Steiner et al. 1998) that could be the energy carrier for the upper atmospheres. With this simple situation, we have performed MHD simulations directly covering from the photosphere to the interplanetary space. About 1,800 minutes after Alfvénic wave is forced to excite, our numerical system has reached quasi-steady state. Because of Alfvénic wave dissipation, the initial static and isothermal (10^4 K) atmospheres have eventually achieved the hot corona (10^6 K) and the high-speed (> 500 km s $^{-1}$) solar wind (Figs. 1 and 2). The radial profiles of velocity, temperature, and density are quite well consistent with observations from spectroscopy and interplanetary scintillation (Fig. 2). Although the similar radial profiles are also shown by the previous one dimensional simulation

(Suzuki & Inutsuka 2005, 2006), heating and accelerating mechanism in our simulation is essentially different from the previous one.

Radiative cooling, thermal conduction loss, and adiabatic cooling due to the solar wind are main cooling processes in the solar atmosphere. In order to maintain the corona, heating processes are necessary to balance with these cooling processes. As shown in the upper panel of figure 3, the energy flux of the Alfvénic wave monotonically decreases, a part of which is transferred to the solar wind. Although a sizable fraction attenuates in the chromosphere by the reflection and dissipation, the supplied flux to the corona is well above $10^5 \text{ erg cm}^{-2} \text{ s}^{-1}$, which is sufficient to maintain the corona and solar wind (Hansteen & Leer 1995). The dissipation mechanism of the Alfvénic wave should be different in region to region according to the background medium.

Lower panel of figure 3 compares each component of the heating and cooling rates. The heating is separated into the compressive (dilatational) and incompressible (shearing) parts. The green solid line shows the compressive component; compressive waves are nonlinearly generated by the mode conversion from the Alfvénic waves (Kudoh & Shibata 1999) and these compressive waves steepen to shocks. We estimate the heating rate by counting the entropy jumps at shock fronts in the simulations. The red-hatched area shows the incompressible heating, which is done by the dissipation of Alfvénic turbulence owing to strong shearing motion at small scales. We estimate the turbulent heating rate from the Fourier component of Alfvénic disturbances.

In the chromosphere, both shock and turbulence contribute to the heating. The wave nonlinearity, which is defined as wave amplitude divided by phase speed, quickly increases in the chromosphere with the rapid expansion of the magnetic flux tube. As a result, compressive waves are effectively generated by the nonlinear mode conversion. The turbulent heating is also comparably important in the chromosphere because the Alfvénic turbulence is efficiently developed by both phase mixing (Heyvaerts & Priest 1983) and wave reflection (Matthaeus et al. 1999). Because the flux tube rapidly opens near the photosphere, the Alfvén speeds of the neighboring field lines are largely different. Then, the Alfvénic waves along the neighboring field lines gradually become out of phase, even though the waves are in phase at the photosphere, which creates strong shear to dissipate their wave energy. In addition, the rapid decrease of the density in the chromosphere and the transition region, and accordingly the change of the Alfvén speed, causes the reflection of the Alfvénic wave. The nonlinear wave-wave interaction between the pre-existing outward component and the reflected component leads to the turbulent cascade to smaller scales.

In the corona, the shock dissipation is the main contributor to the heating although the turbulence is also effective in the coronal bottom. Passing through the transition region, the wave nonlinearity decreases rapidly because of the large Alfvén speed in the corona. Therefore, the local shock formation in the corona is not significant. Instead of that, compressive waves are generated by the vertically fluctuating motion of the transition region; the nonlinearly excited longitudinal waves in the chromosphere

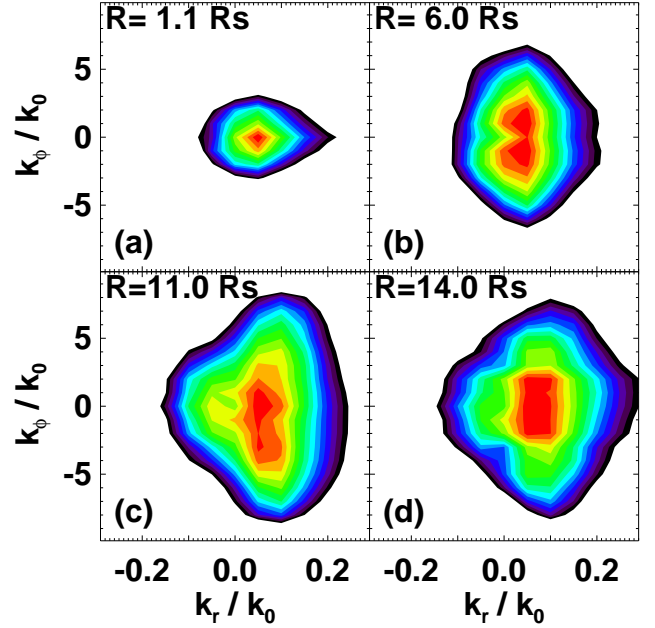


Fig. 4.— Evolution of Alfvénic wave power spectrum with respect to radius. The four panels represent the Alfvénic wave power spectrum at (a) $R=1.1 \text{ Rs}$, (b) $R=6.0 \text{ Rs}$, (c) $R=11 \text{ Rs}$, and (d) $R=14 \text{ Rs}$. The vertical and the horizontal axis represents the wave number in ϕ direction, k_ϕ , and in r direction, k_r , normalized by $k_0 = 2\pi\Delta\phi$, where $\Delta\phi$ is the angular system size in ϕ direction. The color in each panel shows the power spectral density in Fourier space normalized by the peak value.

continuously tap the transition region (Kudoh & Shibata 1999), which further excites upward compressive waves in the corona. The reflection wave component drops off significantly above the transition region (Fig. 4) because the Alfvén speed does not change so much there. Then, the turbulent cascade is suppressed in the subsonic region (1.02 to 3 Rs). The power index of the energy spectral density of Alfvénic disturbance is significantly softer than $-5/3$, which indicates that energy cascading to smaller scales is not effective in this region. The shock heating compensates for the absence of turbulent heating in order to balance with the cooling there. Generally heating below the sonic point controls mass loading to the solar wind. Therefore we suggest that the shock heating mechanism works efficiently to determine the mass loss rate from the sun. In our simulation, mass loss rate is of the order of $10^{-14} \text{ M}_\odot \text{ yr}^{-1}$ which is reasonably well agree with the observed value.

In the solar wind acceleration region, again, both turbulent heating and shock heating are comparably important. The wave nonlinearity, once dropped above the transition region, increases gradually with radius due to the decrease in Alfvén speed. Then, compressive waves are locally excited by the mode conversion, and these waves finally dissipate by shocks. The turbulent heating also effectively works in the solar wind. The signature of turbulent cascade can be clearly seen in power spectra of

Alfvénic waves (Fig. 4). Moreover, the turbulent cascade is not isotropic but anisotropic (Shebalin et al. 1983; Cho & Lazarian 2003); the direction of cascade is perpendicular to the background magnetic field. The energy cascading here is inferred to be triggered by the nonlinear wave-wave interaction between the outgoing and reflection waves (Matthaeus et al. 1999) since the increase of the reflection component of Alfvénic waves can be seen in figure 4. The works done by gas and magnetic pressure from the turbulence also turned out to be the same order of magnitudes and accelerate the solar wind.

Our simulation reveals that both the shock and the turbulence are essential for the coronal heating and the solar wind acceleration. This indicates that the energy exchange between Alfvénic mode and compressive mode is effective, although recent MHD simulations of turbulence in homogeneous media show the decoupling of Alfvénic and compressive modes (Cho & Lazarian 2003). The inhomogeneity of the background medium, namely the density stratification and the rapidly expanding flux tube, is essential to understand the energy transfer processes in the solar atmosphere. In the previous 1D simulations (Suzuki & Inutsuka 2005, 2006), shock heating is considered to be overestimated because the geometrical expansion generally dilutes shocks in multidimensional system. We show that the shock dilution is not so significant in 2D system to exclude the shock-heating model although further investigation for 3D simulation is necessary. While the shock is always main heating and acceleration mechanism, the turbulence has preferred region to develop. We show that these changes in the main contributor to the heating are the natural consequences of the strong inhomogeneity originated both in the photospheric magnetic field and in the gravitational stratification. Although only the Alfvénic disturbances are excited at the photosphere in this study, compressive waves are also important especially for the chromospheric heating (Bogdan et al. 2003; Hasan et al. 2005; Fedun et al. 2011). It is possible to change the reflection rate of Alfvénic wave because the extra heating by compressive waves modifies the density structure around the transition region.

Numerical computations were carried out on Cray XT4 at Center for Computational Astrophysics, CfCA, of National Astronomical Observatory of Japan. Takuma Matsumoto is supported by the Research Fellowship from the Japan Society for the Promotion of Science for Young Scientists.

REFERENCES

Antolin, P., & Shibata, K. 2010, *ApJ*, 712, 494
 Banerjee, D., Teriaca, L., Doyle, J. G., & Wilhelm, K. 1998, *A&A*, 339, 208
 Bogdan, T. J. et al., 2003, *ApJ*, 631, 1270
 Cho, J. & Lazarian, A. 2003, *MNRAS*, 345, 325
 Cranmer, S. R., Van Ballegoijen, A. A., & Edgar, R. J. 2007, *ApJ*, 171, 520
 De Pontieu, B. et al., 2007, *Science*, 318, 1574

Dmitruk, P., & Matthaeus, W. H. 2003, *ApJ*, 597, 1097
 Esser, R. et al., 1999, *ApJ*, 510, L63
 Fedun, V., Shelyag, S., & Erdélyi, R. 2011, *ApJ*, 727, 17
 Fludra, A., Del Zanna, G., & Bromage, B. J. I. 1999, *Space Sci. Rev.*, 87, 185
 Grall, R. R. et al., 1996, *Nature*, 379, 429
 Habbal, S. R., Esser, R., Guhathakurta, M., & Fisher, R. R. 1995, *Geophys. Res. Lett.*, 22, 1465
 Hansteen, V. H., & Leer, E. 1995, *J. Geophys. Res.*, 100, 21577
 Hasan, S. S., Van Ballegoijen, A. A., Kalkofen, W., & Steiner, O. 2005, *ApJ*, 631, 1270
 Heyvaerts, J., & Priest, E. R. 1983, *A&A*, 117, 220
 Kudoh, T., & Shibata, K. 1999, *ApJ*, 514, 493
 Lamy, P. et al., 1997, in *Fifth SOHO Workshop: The Corona and Solar Wind near Minimum Activity*, ed. A. Wilson (ESA SP-404; Noordwijk: ESA), 491
 Matsumoto, T., & Shibata, K. 2010, *ApJ*, 710, 1857
 Matsumoto, T., & Kitai, R. 2010, *ApJ*, 716, L19
 Matthaeus, W. H., Zank, G. P., Oughton, S., Mullan, D. J., & Dmitruk, P. 1999, *ApJ*, 523, L93
 McIntosh, S. W. et al., 2011, *Nature*, 475, 477
 Miyoshi, T., & Kusano, K. 2005, *J. Comput. Phys.*, 208, 2005
 Nishizuka, N. et al., 2008, *ApJ*, 683, L83
 Okamoto, T. J., & De Pontieu, B., 2011, *ApJ*, 736, L24
 Shebalin, J. V., Matthaeus, W. H., & Montgomery, D. 1983, *J. Plasma Phys.*, 29, 525
 Steiner, O., Grossman-Doerth, U., Knöelker, M., & Schüssler, M. 1998, *ApJ*, 495, 468
 Suzuki, T. K., & Inutsuka, S. 2005, *ApJ*, 632, L49
 Suzuki, T. K., & Inutsuka, S. 2006, *J. Geophys. Res.*, 111, A06101
 Teriaca, L., Poletto, G., Romoli, M., & Biesecker, D. A. 2003, *ApJ*, 588, 566
 Tóth, G. 2000, *J. Comput. Phys.*, 161, 605
 Tsuneta S. et al., 2008, *ApJ*, 688, 1374
 Verdini, A., & Velli, M. 2007, *ApJ*, 662, 669
 Wilhelm, K. et al., 1998, *ApJ*, 500, 1023
 Yokoyama, T., & Shibata, K. 2001, *ApJ*, 549, 1160
 Zangrilli, L., Poletto, G., Nicolosi, P., Noci, G., & Romoli, M. 2002, *ApJ*, 574, 477